Journal of Cardiovascular Magnetic Resonance (2006) **8,** 619–631
Copyright © 2006 Taylor & Francis Group, LLC
ISSN: 1097-6647 print / 1532-429X online
DOI: 10.1080/10976640600721510

Taylor & Francis
Taylor & Francis Group

CONGENITAL HEART DISEASE

Simple Congenital Heart Lesions

Rachel M. Wald, MD and Andrew J. Powell, MD

Department of Cardiology, Children's Hospital Boston, Boston, Massachuettes, USA; Department of Pediatrics, Harvard Medical School, Boston, Massachuettes, USA

ABSTRACT

Cardiac magnetic resonance imaging (CMR) can provide comprehensive anatomic and physiological information about the cardiovascular system. The review article describes the application of CMR to several simple congenital heart lesions: atrial septal defects and other interatrial communications, ventricular septal defects, patent ductus arteriosus, partially anomalous pulmonary venous connection, and coarctation of the aorta. The anatomy, clinical features, and management of these lesions are discussed. CMR techniques to evaluate patients with these lesions are described and relevant literature is reviewed.

INTRODUCTION

Technical advances over the past two decades have greatly expanded the diagnostic role of cardiac magnetic resonance imaging (CMR) in patients with congenital heart disease. In addition to high-resolution anatomic information, CMR provides physiological information about the cardiovascular system such as ventricular function and blood flow. Along with these improved capabilities, the speed and efficiency of imaging have also increased thereby allowing a comprehensive examination to be obtained within a time frame acceptable to both patient and operator. This review describes the CMR evaluation of several "simple" congenital heart lesions: atrial septal defect (ASD) and other interatrial communications, ventricular septal defect (VSD), patent ductus arteriosus (PDA), partially anomalous pulmonary venous connection (PAPVC), and coarctation of the aorta. More "complex" lesions are discussed in the following article.

Despite being classified as "simple," many of the conditions in this review have important anatomic subtypes and varying physiology. Thus, summaries of the anatomic considerations and clinical management are provided for each lesion. The supervising physician should have a thorough understanding of these issues, carefully review the patient history, and examine the available imaging data before conducting the examination in order to ensure a high-quality, complete CMR evaluation.

Because young children typically have excellent acoustic windows, echocardiography is usually the primary imaging modality in this age group and is often sufficient alone. However, in older patients or those who have undergone surgery, the echocardiographic evaluation may be incomplete, and CMR is often indicated. CMR may also be useful for these "simple" lesions in selected patients to provide additional quantitative data or to help resolve clinical scenarios in which the data are inconsistent. This utility applies not only to the initial evaluation but also to serial follow-up and post-operative assessment.

Received 2 August 2005; accepted 15 January 2006.
Keywords: Atrial Septal Defects, Ventricular Septal, Patent Ductus Arteriosus, Partially Anomalous Pulmonary Venous Connection.
Correspondence to:
Andrew J. Powell, MD
Department of Cardiology
Children's Hospital Boston
300 Longwood Avenue
Boston, MA 02115
fax: 617-739-3784
e-mail: andrew.powell@cardio.chboston.org

ATRIAL SEPTAL DEFECTS AND OTHER INTERATRIAL COMMUNICATIONS

Anatomy

Anatomically, five different defects can lead to an interatrial shunt (Fig. 1). 1) A patent foramen ovale is bordered on the left by septum primum and by the superior limbic band of the fossa ovalis (septum secundum) on the right. It is an important and nearly universally present communication during fetal life. Following the transition to a postnatal circulation, septum primum opposes the superior limbic band of the fossa ovalis, and the foramen ovale narrows. A patent foramen ovale is seen in almost all newborns and with decreasing frequency throughout life (1). 2) A secundum ASD is the most common cause of an atrial

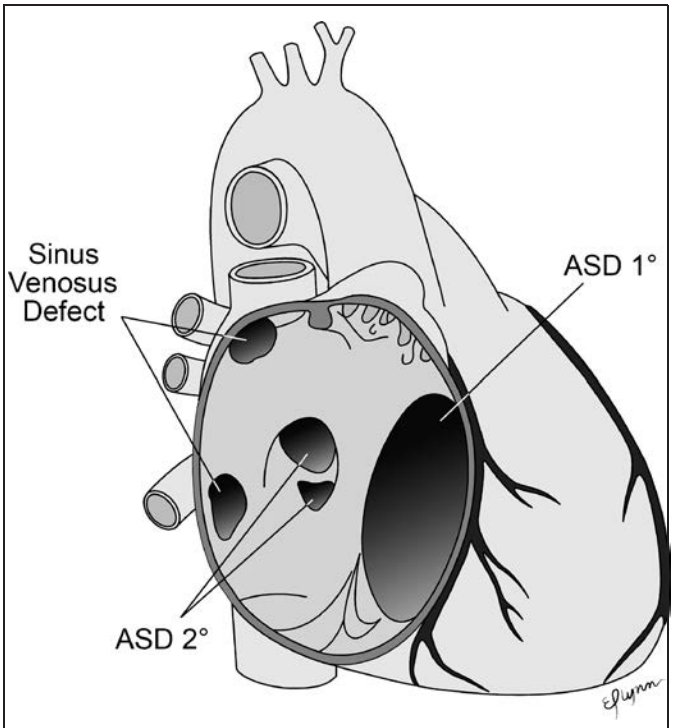

Figure 1. Anatomic types of atrial communications (see text for details). ASD 1° denotes primum atrial septal defect; ASD 2° denotes secundum atrial septal defect.

level shunt after patent foramen ovale. Usually the defect is due to deficiency of septum primum, the valve of the fossa ovalis, but rarely, it results from a deficiency of septum secundum (the muscular limb of the fossa ovalis). The defect may be single or multiple with several fenestrations of septum primum. 3) A primum ASD is a variant of incomplete common atrioventricular canal and is the third most common interatrial communication. This defect involves the septum of the atrioventricular canal and is almost always associated with a cleft anterior mitral leaflet. Any associated defect within the fossa ovale (secundum ASD) is regarded as a separate abnormality. 4) A sinus venosus septal defect results from deficiency of the sinus venosus septum which separates the pulmonary veins from the systemic veins and the sinus venosus component of the right atrium. Most commonly, a sinus venosus defect is between the right upper pulmonary vein and the cardiac end of the superior vena cava. Rarely, the defect involves the right lower and/or middle pulmonary veins and the inferior aspect of the right atrium at its junction with the inferior vena cava. From an anatomic standpoint, a sinus venosus defect is not an ASD because it does not allow direct communication between the left and right atria. Instead, the interatrial flow travels between the left atrium, one or more of the pulmonary veins, the sinus venosus septal defect, the superior (or inferior) vena cava, and the right atrium. The defect usually allows pulmonary vein flow to drain to the right atrium through the defect as well. Patients with sinus venosus defects commonly have additional accessory right upper pulmonary veins which connect to the superior vena cava or azygous vein. 5) A coronary sinus septal defect is a rare type of interatrial communication in which the septum between the coronary sinus and the left atrium is either partially or completely unroofed, allowing the right and left atria to communicate through the defect and the coronary sinus orifice. Sometimes there is also a persistent left superior vena cava draining to the coronary sinus. If the coronary sinus is completely unroofed, the left superior vena cava will appear to be connected to the left atrium. The association of a coronary sinus septal defect and persistent left superior vena cava is termed Raghib syndrome, and may result in cyanosis (2).

Clinical course and management

Regardless of the specific anatomic type, the amount of shunting through an interatrial communication is determined by the defect size and relative compliance of the right and left ventricles. Over the first few months of life, right ventricular compliance typically rises leading to an increasing left-to-right shunt. During adulthood, left ventricular compliance normally decreases further augmenting the left-to-right flow. Shunt flow through the right heart and lungs leads to dilation of the right atrium, right ventricle, pulmonary arteries, and pulmonary veins. Most young children tolerate this increased pulmonary blood flow well and are asymptomatic; a few develop dyspnea or growth failure. Defects in this age group are typically detected after auscultation of a heart murmur or incidentally when an echocardiogram is obtained for other indications. Up to 5–10% of patients with significant left-to-right shunts may develop pulmonary vascular disease by adulthood leading to pulmonary hypertension. Adults with unrepaired atrial septal defects are also at risk for exercise intolerance, atrial arrhythmias, and paradoxical emboli.

In general, current practice is to refer patients for atrial septal defect closure if the patient is symptomatic or the defect results a significant left-to-right shunt. Evidence for the later includes a defect diameter >5 mm, right ventricular dilation, flattening of the ventricular septum in diastole (caused by elevated right ventricular diastolic pressure from the volume load), and a pulmonary-to-systemic flow ratio >1.5–2.0. One must also be aware that smaller secundum ASDs may close spontaneously or become smaller in the first few years of life; thereafter, defects tend to become larger with time. Primum ASDs, sinus venosus septal defects, and coronary sinus septal defects almost never become smaller with time. Although a patent foramen ovale typically produces only a small shunt, closure may be indicated when there is a history consistent with a paradoxical embolus.

All of these defect types can be closed surgically with a very low mortality and morbidity in centers with expertise. The timing of surgery depends on multiple factors including the size of the defect, associated cardiac abnormalities, symptoms, and local experience, but there is rarely a reason to delay surgical closure beyond 3 years of age. Over the past two decades, transcatheter treatment for secundum ASDs and patent foramen ovales by occluding them with various devices has become available at specialized centers. Although device closure is generally favored

over surgical closure for patent foramen ovale, there is yet no consensus on the specific circumstances under which device closure is superior in secundum ASD.

With regard to surgical technique, secundum ASDs are either closed primarily or with a patch. For primum ASDs, the defect is closed with a patch and, in some cases, the associated mitral valve cleft is partially sutured. Sinus venosus septal defects can often be closed by simply placing a patch to reconstruct the missing portion of the sinus venosus septum thereby eliminating interatrial and right pulmonary vein to right atrial flow. In some cases, especially when a right upper pulmonary vein drains relatively high to the superior vena cava, the superior vena cava is transected superior to the anomalous veins and the distal caval end anastomosed to the right atrial appendage. The sinus venosus septal defect is then closed in such a way that the proximal superior vena cava and anomalous veins drain to the left atrium. For a coronary sinus septal defect, the os of the coronary sinus is usually patched closed. If a left superior vena cava is present, it is redirected to the right atrial side either through ligation, when an adequate left innominate vein is present, or via a baffle to the right atrium.

Much less commonly, interatrial flow through the various types of defects is bidirectional or right-to-left. This typically occurs when right ventricular compliance is low as the result of right ventricular outflow tract obstruction or pulmonary hypertension (i.e., increased pulmonary vascular resistance). Right-to-left shunt flow causes cyanosis and its sequelae including exercise intolerance, paradoxical emboli, and polycythemia. Closure of defects in this clinical setting is often contraindicated as it would exacerbate pulmonary hypertension and right heart failure.

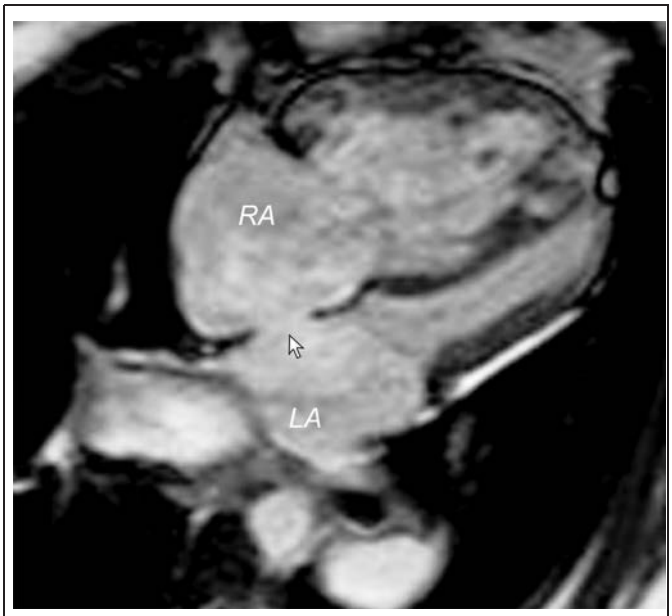

Figure 2. ECG-gated steady state free precession cine MRI in the four-chamber plane showing a secundum atrial septal defect (arrow). Note the dilated right atrium (RA) and right ventricle. LA- left atrium.

MRI evaluation

Transthoracic echocardiography is the primary imaging technique for the evaluation of ASD and is usually sufficient for clinical decision making in the pediatric age range. However, CMR can often be helpful in patients, usually adolescents and adults, with a known or suspected ASD and inconclusive clinical or transthoracic echocardiographic findings. For example, CMR provides a noninvasive alternative to transesophageal echocardiography and to diagnostic catheterization in patients with evidence of right ventricular volume overload in whom transthoracic echocardiography cannot demonstrate the source of the left-to-right shunt. The advent of transcatheter occlusion of ASDs has also increased the need for accurate anatomic information to help determine whether a patient is an appropriate candidate for this intervention versus surgery. In the preintervention situation, the specific goals of the CMR examination include delineation of the location, size, and number of ASDs; evaluation of pulmonary venous return; determination of suitability for transcatheter closure; estimation of right ventricular pressure; and assessment of the hemodynamic burden by quantifying the pulmonary-to-systemic flow (Qp/Qs) ratio, and right ventricular size and systolic function. In patients who have undergone transcatheter device closure of an ASD, additional goals include excluding device malposition, interference with the atrioventricular valves and venous blood flow, thrombus formation, and a residual shunt. Patients who have undergone a repair of a sinus venosus defect are at risk for superior vena cava and right pulmonary vein obstruction. Mitral regurgitation from a residual cleft is often present after primum ASD repair, and should be assessed quantitatively with velocity encoded cine (VEC) MRI.

The anatomic issues should be addressed by acquiring high-resolution images of the atrial septum and adjacent structures including the vena cavae, the pulmonary veins, and the atrioventricular valves. Our preference is to image in at least two planes by acquiring a contiguous stack of locations in the axial or four-chamber plane and a stack in an oblique sagittal plane (Fig. 2). The most useful commonly available techniques for this work are fast (turbo) spin echo and segmented k-space cine steady state free precession pulse sequences, both performed with breath-holding and ECG-gating. Unless image quality is optimal, thin structures such as septum primum may not be clearly demonstrated, leading to an overestimation of the defect's size or to a false positive diagnosis. Moreover, it may be difficult to appreciate the precise anatomy of a secundum ASD with multiple fenestrations. For these reasons, it is also useful to image the atrial septum using VEC MRI both in the plane of the septum to yield an en face view as well as in orthogonal planes planned from the en face view. A non-ECG-gated gadolinium-enhanced three-dimensional magnetic resonance angiogram (3D MRA) sequence is not ideally suited for evaluation of ASDs because of blurring of intracardiac structures from heart motion. However, this technique is helpful in the anatomic evaluation

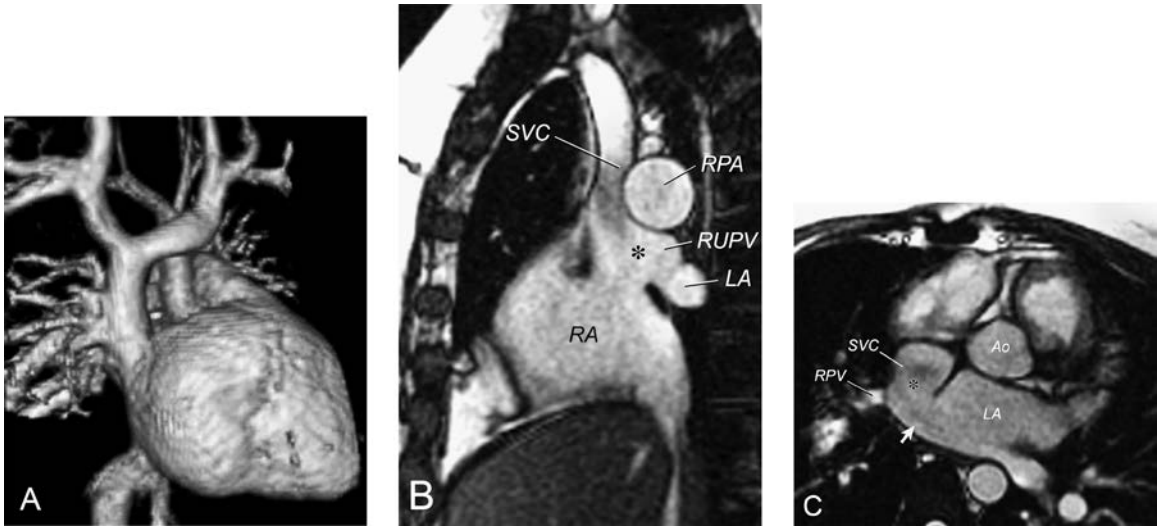

Figure 3. Sinus venosus defect. **A.** Three-dimensional reconstruction of a gadolinium-enhanced 3D MRA showing several pulmonary veins from the right upper lobe draining into the superior vena cava. **B.** ECG-gated steady state free precession cine MR in the sagittal plane showing the defect (*) between the right upper pulmonary vein (RUPV) and the superior vena cava (SVC). **C.** ECG-gated steady state free precession cine MRI in the axial plane showing the defect between the RUPV and the SVC (*). The arrow points to the left atrial orifice of the RUPV. Left-to-right shunt results from drainage of the RUPV to the SVC and from left atrial blood entering the right atrium (RA) through the orifice of the RUPV (arrow) and the unroofed wall between the RUPV and the SVC (*). Ao- ascending aorta; LA-left atrium.

of the pulmonary veins, especially in patients with sinus venosus septal defects which invariably involve the pulmonary veins (Fig. 3).

In patients with known or suspected ASDs, left and right ventricular size and systolic function should be quantified by acquiring a stack of cine steady state free precession images in a ventricular short axis plane. This image series also allows one to make a qualitative estimate of right ventricular systolic pressure based on the configuration of the ventricular septum. The septal geometry is concave towards the right ventricle when the right ventricle-to-left ventricle pressure ratio is low and assumes a flat configuration, or even a concave shape towards the left ventricle, as the right ventricle-to-left ventricle pressure ratio increases. Interpretation of the septal configuration may be confounded by factors such as dysynchronus contraction of the right ventricle, intraventricular conduction delay (e.g., right or left bundle branch block, pre-excitation), and a high left ventricular pressure.

Measurement of the Qp/Qs ratio is clinically useful in patients with ASDs. Multiple studies have shown that VEC MRI calculation of the Qp/Qs ratio by measuring flow in the main pulmonary artery (Qp) and ascending aorta (Qs) agrees closely with catheterization-based oximetry measurements of Qp/Qs (3–6). In the absence of significant valve regurgitation or an additional shunt, Qp/Qs can also be derived from the right (Qp) and left (Qs) ventricular stroke volumes calculated from the short axis cine stack of the ventricles. In clinical practice, it is recommended to measure the Qp/Qs ratio by both of these methods and check the data for consistency.

In addition to case reports, several studies have assessed the role of CMR in evaluating ASDs. Early reports utilized conventional spin echo imaging to compare the apparent defect size with measurements made at surgery and yielded generally good agreement (7–9). Subsequently, Holmvang et al. evaluated defect size by performing VEC MRI carefully positioned in the plane of the ASD to visualize the defect en face (10). These measurements agreed closely with those made at surgery or with balloon sizing at catheterization in 30 patients, mostly adults. However, measurements from conventional spin echo imaging in planes perpendicular to the ASD overestimated the defect size; the discrepancy was attributed to "signal dropout" in the thin portion of the septum.

More recently, Beerbaum et al. studied 65 children with clinically suspected ASDs and inconclusive transthoracic echocardiogram results (11). Defect size and rim measurements were assessed using velocity encoded cine MRI oriented in the ASD plane for en face visualization and in orthogonal planes for the distance to adjacent structures. Time-of-flight angiography was also performed to assess systemic and pulmonary venous return. Based on the CMR examination findings, 30 patients underwent transcatheter device closure and accompanying transesophageal echocardiography. Five of these patients were subsequently referred for surgery because stretched-balloon sizing revealed an unexpectedly large defect. The other 35 children were referred directly to surgery because the defect was deemed unsuitable for device closure or there was associated partial anomalous pulmonary venous return. The accuracy of this determination was confirmed in all cases at surgery. Defect size measurements by CMR agreed well with those by transesophageal echocardiography and at surgery. Rim distances to adjacent structures agreed less well but were usually within 5 mm. The CMR measurement of septal length was larger than that by transesophageal

echocardiography but agreed with surgical results. Rim distance to the coronary sinus and minor septal fenestrations <1 mm were difficult to identify by CMR. All 9 patients with multiple hemodynamically relevant ASDs were correctly diagnosed by en face phase contrast imaging and all 4 patients with partially anomalous pulmonary venous return were accurately identified by time-of-flight angiography. The authors conclude that in children with suspected ASDs and inconclusive transthoracic echocardiograms, CMR is useful for the determination of ASD size, rim distances, and venous connections.

In another recent study, Durongpisitkul et al. reported on 66 children and adults with secundum ASDs who underwent transthoracic echocardiography, transesophageal echocardiography, and CMR to evaluate their suitability for Amplatzer device closure (12). Compared with transesophageal echocardiography, the major axis ASD diameter was significantly larger by CMR (30 $\pm$ 3.9 mm versus 24.4 $\pm$ 3 mm, $p = 0.021$) and correlated better with ASD balloon stretched diameter measured at catheterization. The authors also noted that the posterior inferior ASD rim was not seen adequately in 10 patients by transesophageal echocardiography but could be visualized well in all patients by CMR. Based on these two advantages, the authors suggest that CMR may be more useful than transesophageal echocardiography to assess suitability for Amplatzer device closure.

The application of CMR to diagnose patent foramen ovale in adults suspected of having a paradoxical embolism is now under evaluation by several CMR laboratories. In the most common technique, the atria and pulmonary veins are imaged rapidly (gradient echo with echo planar imaging) during the infusion of gadolinium contrast while the patient performs a Valsalva maneuver. The appearance of contrast in the left atrium after the right atrium but prior to the pulmonary veins indicates a patent foramen ovale. A pilot study using this approach correctly categorized all 15 patients with a patent foramen ovale and all 5 without a patent foramen ovale (13). The 3 patients with atrial septal aneurysms were also appropriately diagnosed; however, the study did not evaluate the accuracy of CMR to identify left atrial thrombus, often a pertinent question in patients suspected of having embolic events.

VENTRICULAR SEPTAL DEFECT

Anatomy

A VSD is a communication between the right and left ventricles through an opening in the ventricular septum. It is one of the most common forms of congenital heart disease and is found frequently in association with complex heart disease. This section will focus on isolated or multiple VSDs in the absence of complex congenital heart disease.

Several VSD anatomic classification systems are in use. Fig. 4 shows the anatomic location of VSDs modified from Van Praagh et al. which includes the following: 1) defects at the junction between the conal septum and the muscular septum which may be confined to the membranous portion (referred to as membranous or perimembranous defects) or be associated with malalignment of the conal septum (conoventricular defects), 2) defects in the muscular septum (called muscular or trabecular defects), 3) defects in the inlet septum (known as atrioventricular canal-type or inlet defects), and 4) defects in the outlet septum (variably called outlet, doubly committed subarterial, subpulmonary, conal septal or supracristal defects) (14).

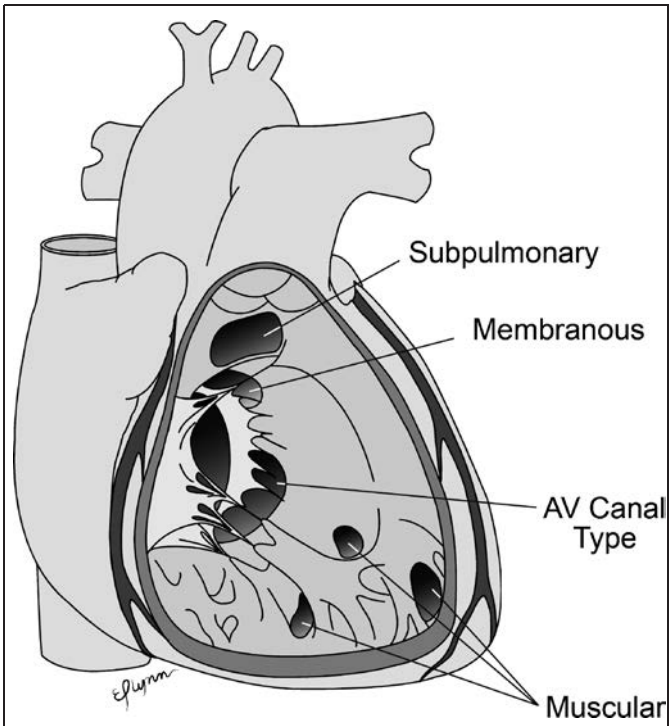

Figure 4. Anatomic types of ventricular septal defects (see text for details).

Clinical course and management

The natural history of a VSD is related to the size and location of the defect. Defects in the membranous or muscular septum often become smaller over time and may spontaneously close. In contrast, malalignment conoventricular defects, outlet septum defects, and atrioventricular canal-type defects are usually large and remain so. Consequently, such patients often undergo surgical closure in infancy. Venturi effects associated with VSDs in the membranous or outlet septum may cause aortic valve leaflets (usually the right coronary cusp) to prolapse through the defect. Although the leaflet prolapse typically reduces the effective orifice size of the defect, it may also lead to aortic insufficiency. VSDs, particularly those associated with turbulent flow jets, also predispose patients to the development of endocarditis.

Symptoms are predominantly determined by the size of the shunt through the VSD which, in turn, is related to the defect size and the relative resistances of the pulmonary vascular and the systemic vascular beds. In most situations, pulmonary resistance is lower than systemic resistance, and there is a left-to-right shunt. The resulting increased blood flow to the lungs and left

heart may lead to dilation of the pulmonary arteries, pulmonary veins, left atrium, and left ventricle. Because most of the shunt flow passes through the VSD into the right ventricle in systole, right ventricular dilation is usually not present. If the shunt is small, the patient is asymptomatic, and intervention to close the defect is not warranted. When the shunt is large, symptoms from pulmonary overcirculation (e.g., tachypnea, diaphoresis, poor feeding, and slow weight gain) may develop in the first few months of life. If the defect is unlikely to become small over time or if these symptoms cannot be managed medically, surgical closure in infancy is recommended. Untreated, patients with VSDs and large left-to-right shunts may develop irreversible pulmonary hypertension from elevated pulmonary vascular resistance. In such cases, the flow through the defect will become increasing right-to-left resulting in cyanosis (Eisenmenger syndrome). Occasionally, one may encounter older patients with intermediate-sized VSDs who are minimally symptomatic and have normal pulmonary artery pressure yet have a large enough shunt to result in left ventricular dilation. VSD closure is probably warranted under these circumstances given its low risk and the potential beneficial impact on ventricular function long-term.

A surgical approach is by far the most common technique used to close VSDs and carries a low mortality even when performed in the first few months of life (15). Typically the surgeon works through the tricuspid valve and applies a patch to cover the defect. Experience with transcatheter delivery of occlusion devices is growing and this approach may be appropriate in selected circumstances (16, 17).

MRI evaluation

Transthoracic echocardiography is the primary diagnostic imaging modality in patients with suspected or known VSDs and is usually adequate. Occasionally in larger patients, acoustic windows may be insufficient, and CMR is indicated to define the defect size and location as well as identify associated conditions such as aortic valve prolapse. CMR may also be of use when the hemodynamic burden of a defect is uncertain by providing reliable quantitative data on the Qp/Qs ratio, and ventricular dimensions and function.

VSD location and size can be demonstrated by cine gradient echo (preferably steady state free precession) or spin echo sequences (18–20). Very small defects may be difficult to resolve; however, the associated turbulent flow can be made quite conspicuous on gradient echo sequences provided the echo time is long enough to allow for sufficient spin dephasing (Fig. 5). It is useful to assess the ventricular septum using stacks of images oriented in at least two planes. The four-chamber plane provides base-to-apex localization whereas the short-axis plane shows the location in the anterior-to-posterior axis (Fig. 6). Additional imaging in other planes can be used as needed to demonstrate defect position relative to key adjacent structures (e.g., atrioventricular or semilunar valves). Bremerich and colleagues have reported that CMR is an important, non-invasive test in the diagnosis and management of defects in the outlet septum as echocardiography was unable to adequately image this region of the ventricular septum (21). Yoo and colleagues demonstrated how CMR can provide an en face view of a VSD,

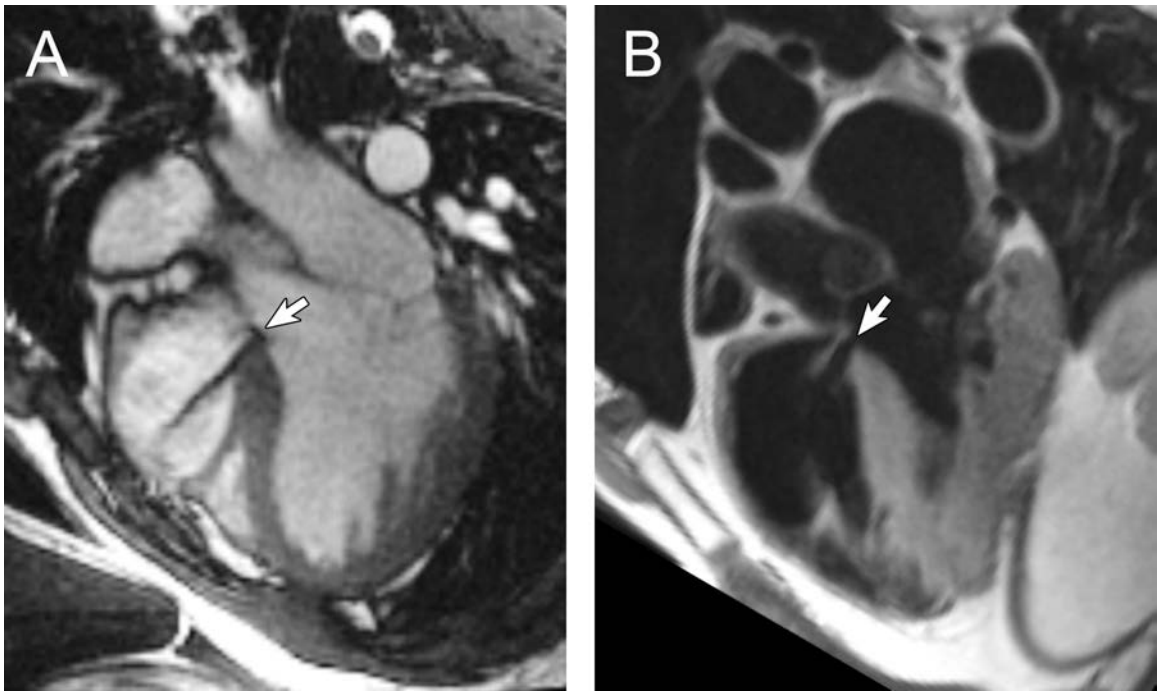

Figure 5. Membranous ventricular septal defect (arrow). **A.** ECG-gated steady state free precession cine MRI in a four-chamber plane showing the defect and associated flow jet into the right ventricle. **B.** ECG-gated fast spin echo image in a four-chamber plane.

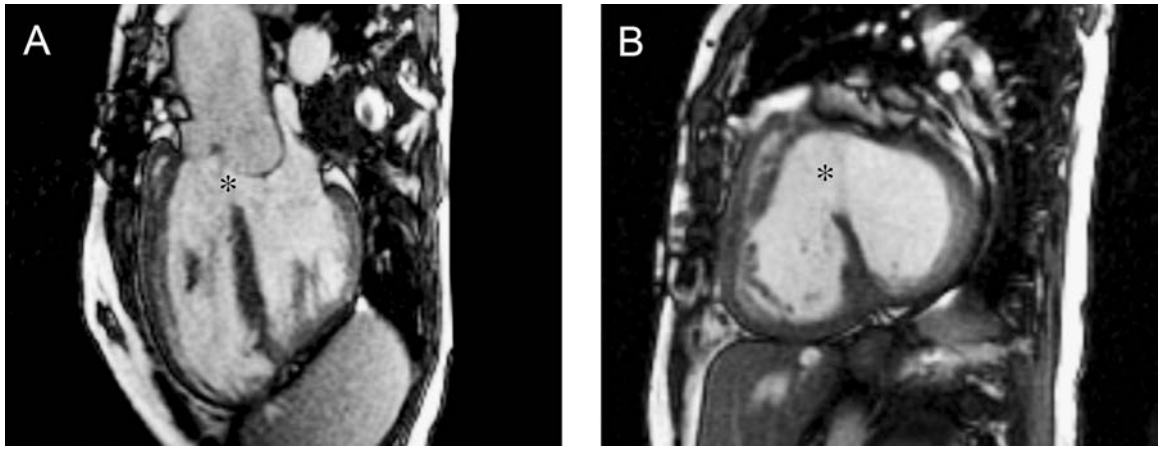

Figure 6. Malalignment conoventricular septal defect (*) imaged with ECG-gated steady state free precession cine MRI in ventricular long-axis (**A**) and short-axis (**B**).

which is particularly advantageous in complex anatomy, such as double inlet ventricle with transposed great arteries in which systemic blood flow is dependent on passage through the defect (22, 23). Recently, an ECG and navigator-gated isotropic three-dimensional steady-state free precession sequence was developed to assess intracardiac anatomy in patients with congenital heart disease. The resulting high-resolution block of anatomic data can be reformatted in multiple planes to characterize VSDs and other abnormalities (24). Image quality with this approach, however, was significantly worse in younger patients (approximately <7 years).

Measurement of ventricular dimensions and function is also key element of the CMR evaluation in a patient with a VSD. This can be done from the ventricular short-axis cine MRI image stack mentioned above. Larger left-to-right shunts will result in left ventricular dilation but not right ventricular dilation. Ventricular systolic function is usually normal. As described in the section on ASDs above, ventricular septal configuration can be used to estimate right ventricular pressure. Finally, quantification of the VSD shunt should be performed by calculating the Qp/Qs ratio. This can be accomplished by measuring the net blood flow in the main pulmonary artery (Qp) and the ascending aorta (Qs) using VEC MRI (4, 6, 25). Alternatively, in the absence of significant valve regurgitation or other shunts, the ventricular volumetric data can be used. The Qp/Qs ratio is equal to right ventricular stroke volume divided by left ventricular stroke volume. In practice, both approaches are recommended and the two results should be checked for consistency.

PATENT DUCTUS ARTERIOSUS

Anatomy, clinical course, and management

The ductus arteriosus is a vascular channel that usually connects the aortic isthmus with the origin of either the left or the right pulmonary artery. During fetal life, the ductus arteriosus allows the majority of the right ventricular output to bypass the lungs by carrying blood flow to the descending aorta. Normally, the ductus arteriosus closes shortly after birth. It may persist in patients with congenital heart disease allowing communication between the systemic and pulmonary circulations. A persistent PDA is common in premature infants and is associated with increased morbidity. In full-term infants and children, the clinical course and sequelae of an isolated PDA are usually related to the ductus size and the direction of flow. In the absence of elevated pulmonary vascular resistance, isolated PDAs have left-to-right flow leading to increased pulmonary flow, and a volume load to the left heart. Larger PDAs cause a significant left-to-right shunt and, if untreated, lead to pulmonary overcirculation, respiratory distress, growth failure, and eventually pulmonary vascular disease. Smaller ducts place the patient at risk for infective endarteritis. Thus in the absence of elevated pulmonary vascular resistance, most isolated persistent PDAs should be closed. This can be accomplished either surgically or in the catheterization laboratory using occluding devices.

MRI evaluation

CMR is seldom requested primarily for assessment of an isolated PDA as this usually presents in childhood and is a straight-forward echocardiographic diagnosis. In several types of complex congenital heart disease, evaluation of the ductus arteriosus is an important element of the examination. For example, in patients with tetralogy of Fallot and pulmonary atresia, the ductus arteriosus may persist and can be an important source of pulmonary blood supply. Gadolinium-enhanced 3D MRA is a particularly helpful imaging technique in these patients because it allows accurate delineation of all sources of pulmonary blood supply, including a PDA, aorto-pulmonary collaterals, and the central pulmonary arteries (Fig. 7) (26). Cine MRI is also useful in detecting PDAs, particularly those which are small with turbulent flow. As with VSD jets, a longer TE will allow more time for spin dephasing and make the turbulent flow more conspicuous. When a PDA is detected, VEC MRI is useful to evaluate the

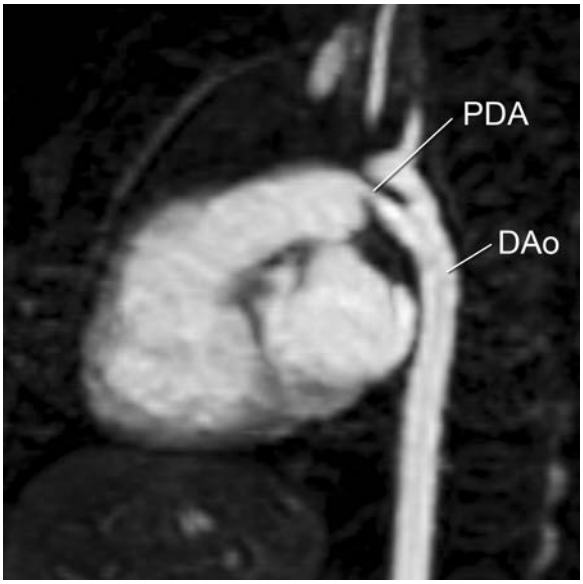

Figure 7. Gadolinium-enhanced 3D MRA (oblique sagittal subvolume maximal intensity projection) in an infant illustrating a patent ductus arteriosus (PDA). DAo-descending aorta.

direction of flow across the ductus and quantify the Qp/Qs ratio. Note that with a PDA and no other shunting lesions, systemic flow (Qs) is equal to the main pulmonary artery flow, and pulmonary flow (Qp) is equal to ascending aorta flow. In patients with a PDA, it is also helpful to measure ventricular volumes and function, and assess right ventricular pressure by evaluating ventricular septal position in systole.

PARTIALLY ANOMALOUS PULMONARY VENOUS CONNECTION

Anatomy

In PAPVC, one or more but not all of the pulmonary veins connect to a systemic vein. PAPVC may be seen in isolation or as a component in complex congenital heart lesions, particularly heterotaxy syndrome with polysplenia. There is wide variability in the number of abnormal veins, the site of their termination, and the caliber of the associated connecting vessels. A detailed description of the variety of lesions captured by this diagnosis may be found elsewhere (27). Common PAPVC types include anomalous connection to the left innominate vein, to the right superior vena cava, to the azygous vein, or to the inferior vena cava. Anomalous connection of some or all of the right pulmonary veins to the inferior vena cava is termed *scimitar syndrome*. The name is derived from the curvilinear shadow in the right lung on chest radiography caused by the anomalous vein as it descends towards the right hemidiaphragm which resembles a scimitar, or Turkish sword. Other abnormalities commonly seen in scimitar syndrome include hypoplasia of the right lung and pulmonary artery, secondary dextrocardia, and anomalous systemic arterial supply usually from the descending aorta to the right lung (28).

Clinical course and management

PAPVC results in a left-to-right shunt: blood draining from the lungs returns to the lungs via the systemic veins and right heart without passing through the systemic arterial circulation. This physiology leads to increased pulmonary blood flow and resembles that of an ASD. The magnitude of the shunt is determined by the number of involved veins, the site of their connections, the pulmonary vascular resistance, and the presence of associated defects. Dilation is commonly seen in the systemic veins downstream of the anomalous pulmonary vein insertion site, the right atrium and ventricle, and the pulmonary arteries. Young patients are usually asymptomatic; dyspnea on exertion becomes increasingly common in the third and fourth decades of life. Development of pulmonary hypertension is very rare. Patients may come to attention after auscultation of a pulmonary flow murmur or when diagnostic imaging is performed for another indication. Evidence of right ventricular volume overload with no apparent intracardiac shunt should prompt a search for PAPVC. The presentation of Scimitar syndrome varies widely depending on the severity of the associated abnormalities. Infants may be critically ill with respiratory compromise while adults may have minimal symptoms. Pulmonary hypertension may develop from a combination of stenosis of the pulmonary veins, arterial blood supply from the descending aorta, pulmonary hypoplasia and parenchymal pulmonary abnormalities.

For the most part, anomalous veins can be surgically corrected, but the likelihood of success and probable benefits must be weighed carefully. A single small anomalous pulmonary vein is associated with a modest left-to-right shunt and does not require intervention. In those with much or all of the left pulmonary veins returning to the left innominate vein, the connecting vertical vein is usually large and long enough to detach from the innominate vein and anastomose to the left atrium. For veins connecting to the superior vena cava, a baffle within the superior vena cava and across the atrial septum can be constructed to channel the pulmonary venous return to the left atrium. Alternatively, the superior vena cava can be transected superior to the anomalous veins and the caval end anastomosed to the right atrial appendage. A baffle across the atrial septum is then created to direct the pulmonary venous flow in cardiac end of the superior vena cava to the left atrium. Pulmonary veins entering the inferior vena cava can be baffled successfully to the left atrium. The most common post-operative complications seen in patients with PAPVC correction are obstruction and residual leaks in the created channels.

MRI evaluation

If a clinical concern for PAPVC cannot be resolved by echocardiography with confidence, MRI is the most appropriate additional diagnostic imaging test. The acoustic properties of lung tissue may make it difficult by echocardiography to trace possible anomalous veins back into the lungs to confirm that they are pulmonary rather than systemic veins. This limitation it not encountered with CMR.

Figure 8. Gadolinium-enhanced 3D MRA (oblique coronal subvolume maximal intensity projection) illustrating partially anomalous pulmonary venous connection of the left upper pulmonary vein (arrow) to the left innominate vein.

Figure 9. Gadolinium-enhanced 3D MRA (oblique coronal subvolume maximal intensity projection) in an adult with scimitar syndrome.

The goals of CMR evaluation of PAPVC include precise delineation of the anatomy and quantification of the imposed hemodynamic burden. Gadolinium-enhanced 3D MRA is an effective and efficient technique to define the thoracic vasculature anatomy including the pulmonary veins, pulmonary arteries, and aortopulmonary collateral vessels (Figs. 8 and 9). The image data set can be reformatted in any plane to illustrate spatial relationships and has sufficient resolution to detect vessels <1 mm. For added confidence, additional imaging of the vascular anatomy can be obtained using cine gradient echo or fast spin echo with blood signal nulling sequences.

Several studies assessing the accuracy and utility of gadolinium-enhanced 3D MRA have shown similar results (29–31). They found a high level of agreement between findings on MR angiography compared with surgical inspection and x-ray angiography. MR angiography was uniformly more accurate than transthoracic and transesophageal echocardiography. CMR studies often diagnosed previously unknown PAPVC or added new clinically important information regarding PAPVC anatomy.

Patients with PAPVC should also have their ventricular dimensions and function measured using a stack of cine MRI oriented in the ventricular short-axis plane. Particular attention should be devoted to quantifying right ventricular end-diastolic volume as this should be related to the size of the left-to-right shunt. The shunt should also be measured directly by obtaining VEC MRI flow measurements in the main pulmonary artery (Qp) and the ascending aorta (Qs). In some cases it may also be possible to measure the flow in the anomalously draining vein itself. In the absence of significant valvular insufficiency, the ventricular stoke volume differential should also be equal to the shunt size and thus serves as a useful check. It is worth noting that in patients with PAPVC, Qp/Qs ratio measurements by oximetry in the catheterization laboratory are inherently inaccurate because of the difficulty in obtaining a reliable, representative mixed systemic venous saturation. Because blood flow is measured directly, these concerns do not apply to MRI measurements. In cases where there is a hypoplastic pulmonary artery or pulmonary venous pathway obstruction, it is also useful to calculate differential pulmonary blood flow using VEC MRI measurements in the branch pulmonary arteries.

COARCTATION OF THE AORTA

Anatomy

Coarctation of the aorta is a discrete narrowing most commonly located just distal to the left subclavian artery, at the site of insertion of the ductus arteriosus. It is thought to arise either from an abnormal flow pattern through the arch during development or from extension of ductal tissue into the aortic wall. Hypoplasia and elongation of the distal transverse arch is a frequent association. Coarctation may be present alone or in combination with other heart lesions including bicuspid aortic valve (the most frequent intracardiac defect), aortic stenosis (valvar or subvalvar), mitral valve abnormalities, ASD, VSD, persistent PDA, and conotruncal anomalies (32, 33).

Clinical course and management

Infants tend to present with symptoms of heart failure and systemic hypoperfusion as the ductus arteriosus closes and, if untreated, may progress to shock or death. Older children and adults typically have isolated coarctation and are usually relatively asymptomatic. A heart murmur, systemic hypertension, or rib notching on a chest x-ray from collateral vessels often leads to the diagnosis. Even in asymptomatic patients, relief of the aortic obstruction is indicated for hemodynamically significant lesions because of the high rate of late complications including congestive heart failure, systemic hypertension, premature coronary artery disease, ruptured aortic or cerebral aneurysms, stroke, aortic dissection, infective endarteritis and premature death (34).

Therapeutic options for coarctation include surgical repair and percutaneous balloon angioplasty, sometimes with stent placement. Currently, resection of the coarctation with an end-to-end anastomosis and augmentation of the transverse arch if needed is the most widely practiced surgical repair and has the lowest incidence of recurrent obstruction. Other approaches have included subclavian flap aortoplasty, patch augmentation, and conduit interposition. These latter techniques have fallen out of favor as post-operative complications, such as aneurysm formation at the site of the prosthetic patch and recurrent arch obstruction, have become increasingly recognized (35, 36). Coarctation in infants is treated surgically in the majority of centers because of the lower risk of residual obstruction or recurrence compared with percutaneous interventions (37). For isolated coarctation, the surgical mortality approaches zero (38). In the event of recurrent coarctation following surgical repair, balloon angioplasty with or without stent placement is often the first line of therapy. Coarctation in older children or adults is increasingly being treated primarily by percutaneous interventions which thus far have shown a low risk of recoarctation and aneurysm formation (39, 40).

MRI evaluation

Transthoracic echocardiography is usually the only diagnostic imaging needed for evaluation of young children with suspected coarctation or following intervention for coarctation. With increasing age, acoustic windows typically deteriorate leading to an incomplete anatomic assessment by echocardiography. In these circumstances, CMR is able to provide high quality anatomic imaging of the aortic arch in its entirety, an assessment of the hemodynamic severity of the obstruction, and evaluation of left ventricular mass and function. In a retrospective study of 84 adult patients following intervention for coarctation of the aorta, Therrien and colleagues showed that the combination of clinical assessment and CMR on every patient was more "cost-effective" for detecting complications than combinations that relied on echocardiography or chest radiography as imaging modalities (41). Other studies have shown the utility of CMR in infants and children with coarctation and other anomalies of the aortic arch (42–44). Computer tomography can also provide excellent anatomic imaging of the aorta but little functional information regarding the left ventricle or pressure gradient across any obstruction. It has the additional disadvantage of ionizing radiation exposure making it a less attractive modality for serial follow-up.

A comprehensive CMR evaluation of patients with suspected coarctation or following intervention for coarctation includes assessment or aortic anatomy; cine MRI sequences to measure ventricular size, function, and mass; and velocity encoded cine MRI sequences to evaluate the severity of obstruction. With regard to aortic anatomy, attention should be given to transverse aortic arch and isthmus, the brachiocephalic vessels, collateral vessels that may bypass obstruction, and possible aneurysms or dissections at the repair sites. Abnormal vessels should ideally be measured in cross-section as elliptical segments are common. If a coarctation is present, its diameter, length, and distance to neighboring vessels should be reported as this may influence decisions regarding percutaneous intervention. Given the association of bicuspid aortic valve with coarctation, the aortic valve morphology should be noted as well as the dimensions of the aortic root and ascending aorta.

Gadolinium-enhanced 3D MRA is an efficient technique to assess aortic anatomy (Fig. 10). Using subvolume maximal intensity projections and reformatting, most of the relevant issues can be addressed and measurements performed (45–48). Cine gradient echo imaging of the aortic arch in long-axis is useful to identify the sites of obstruction because the associated high-velocity turbulent jets produce systolic signal voids. Cine MRI is also helpful for assessment of the aortic valve morphology and aortic root dimensions. Finally, turbo spin echo sequences with nulling of the blood signal can be used to produce high-resolution, high-contrast images of the aorta. They are particularly valuable following endovascular stent placement because there is less metallic susceptibility artifact than with gradient echo sequences. For anatomic definition of the coarctation site, multiple investigators have demonstrated good correlation between these various CMR imaging techniques and X-ray angiography (49–55).

MRI evaluation of coarctation should also include calculation of left ventricular dimensions, systolic function, mass, and mass-to-volume ratio by acquiring a stack of cine steady state free precession images in a ventricular short axis plane. This data is clinically relevant because hypertension is often present and may lead to ventricular hypertrophy and dysfunction. Upper body hypertension may be caused by aortic arch obstruction but systemic hypertension is also prevalent following coarctation repair even without residual coarctation, particularly in patients who had surgery later in life. It is good practice to measure upper and lower extremity cuff blood pressures at the time of the CMR examination to help identify patients with hypertension and estimate the pressure gradient across any aortic obstruction. Note that there may be little upper-to-lower extremity blood pressure differential even with important aortic obstruction when there is a significant collateral circulation bypassing the obstruction.

VEC MRI measurements have been used to gain insight into the functional significance of an obstruction. One approach has been to assess the flow pattern in the descending aorta distal to the coacrtation. Flow characteristics suggestive

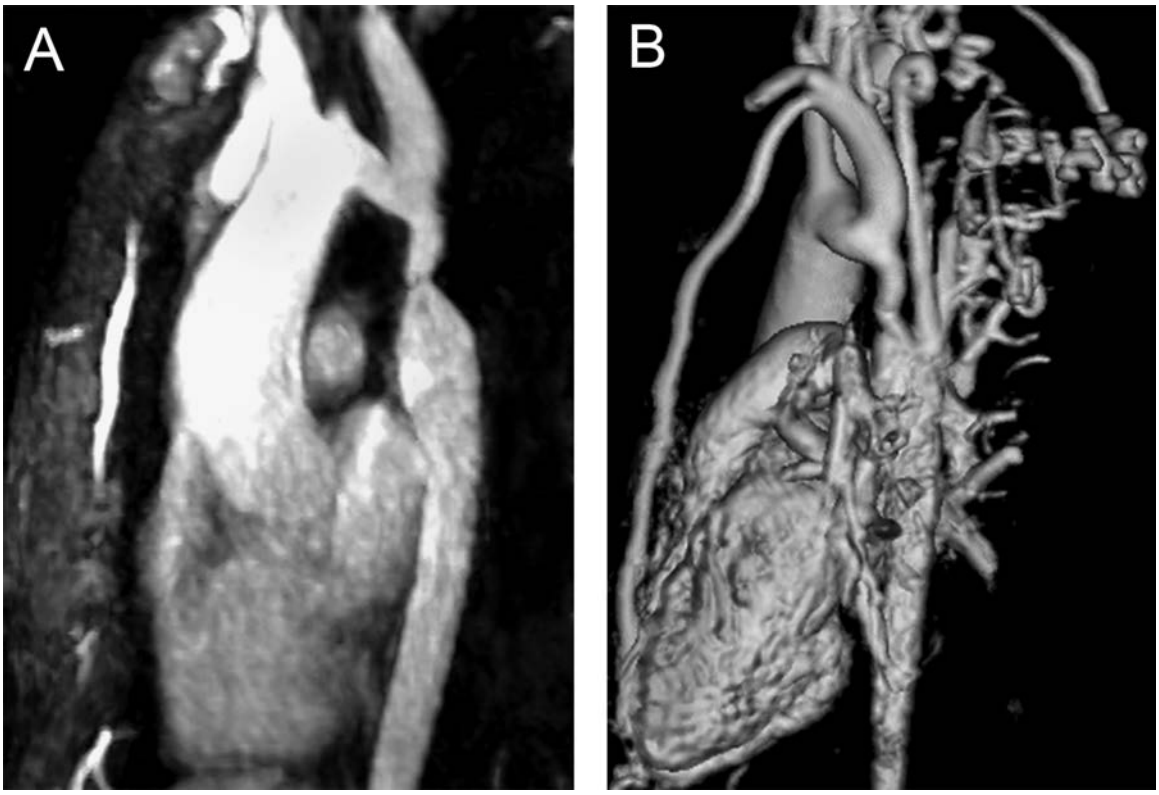

Figure 10. Gadolinium-enhanced 3D MRA. **A**. Oblique sagittal subvolume maximal intensity projection showing elongation of the distal transverse arch, hypoplastic aortic isthmus with severe discrete coarctation at the junction between the isthmus and descending thoracic aorta; **B**. Volume reconstruction shows the coarctation as well as several large tortuous collateral vessels and a dilated left internal mammary artery.

of a hemodynamically significant coarctation include decreased peak flow, decreased time averaged flow, delayed onset of descending aorta flow compared with the onset of flow in the ascending aorta, decreased acceleration rate, and prolonged deceleration with increased antegrade diastolic flow (51, 56, 57). Recently, a model to predict the probability of a hemodynamically significant coarctation pressure gradient (defined as $\geq$20 mm Hg measured during cardiac catheterization) was developed at our institution (58). A combination of the smallest cross-sectional area of the aorta (measured from the gadolinium-enhanced 3D MRA) and the heart rate-adjusted mean deceleration of flow in the descending aorta (measured by VEC MRI distal to the coarctation) predicted a gradient $\geq$20 mm Hg with 95% sensitivity and 82% specificity, 90% positive and negative predictive values, and an area under the receiver-operator characteristics curve of 0.94.

Another approach to assessing severity is to measure the peak coarctation jet velocity and estimate a pressure gradient using the modified Bernoulli equation. Mohiaddin et al. compared peak coarctation jet velocity measured by VEC MRI with that obtained by continuous-wave Doppler and found a high correlation ($r = 0.95$) as well as close agreement (mean difference $= 0.12 \pm 0.23$ m/s) (56). Nevertheless, they note that such measurements are technically difficult in a long, tortuous coarctation segment and that such pressure estimates may not be indicative of anatomic severity because of collateral flow. In support of the latter notion, they found a poor inverse correlation between peak coarctation jet velocity and coarctation diameter ($r = -0.48$). Consequently, they performed additional VEC MRI flow measurements in the ascending and descending aorta distal to the coarctation. Compared to controls, coarctation patients had a significantly lower descending to ascending aorta flow ratio as well as a smaller, more blunted descending aortic flow profile. Similarly, Steffens et al. found that although there was close correlation between gradients obtained by VEC MRI and Doppler echocardiography ($r = 0.95$), both methods showed poorer correlation with cuff blood pressure gradients ($r = 0.63$ for Doppler echocardiography and $r = 0.54$ for PVC MRI) (57). In an effort to improve accuracy, Oshinski et al. proposed that the Bernoulli equation be adapted to take into account hemodynamic variables associated with stenosis severity (59).

Finally, in coarctation patients, VEC MRI has been used to quantify collateral flow entering the descending aorta distal to the obstruction via retrograde flow from the intercostal arteries or vessels arising off the aortic arch and arch branches (57, 60–62). Increased collateral flow suggests more severe obstruction. Moreover, higher collateral flow would be expected to decrease the likelihood of spinal cord ischemic injury during surgical correction which involves interruption of aortic flow. If little collateral flow is suspected, the surgeon may elect to perform left

heart bypass to the descending aorta during the repair. Steffens et al. attempted to directly quantify collateral flow entering the descending aorta via retrograde flow from the intercostal arteries by performing flow measurements slightly distal to the coarctation site and at the level of the diaphragm (57). Total flow from proximal to distal descending aorta decreased by $7 \pm 6\%$ in normal volunteers compared to an increase of $83 \pm 50\%$ in patients with moderate-to-severe coarctation ($p < 0.01$). The amount of flow increase in the distal aorta correlated directly with the severity of anatomic narrowing ($r = 0.94$) and the extremity cuff blood pressure gradient ($r = 0.84$). Nevertheless, the added clinical benefit of this approach is unclear since the extent of collateral flow necessitating left heart bypass to prevent spinal cord ischemic injury during surgical correction has not been defined.

REFERENCES

1. Hagen PT, Scholz DG, Edwards WD. Incidence and size of patent foramen ovale during the first 10 decades of life: an autopsy study of 965 normal hearts. Mayo Clin Proc 1984;59:17–20.
2. Raghib G, Ruttenberg HD, Anderson RC, Amplatz K, Adams P, Jr., Edwards JE. Termination of the left superior vena cava in left atrium, atrial septal defect, and absence of coronary sinus; a developmental complex. Circulation 1965;31:906–18.
3. Powell AJ, Tsai-Goodman B, Prakash A, Greil GF, Geva T. Comparison between phase-velocity cine magnetic resonance imaging and invasive oximetry for quantification of atrial shunts. Am J Cardiol 2003;91:1523–5.
4. Beerbaum P, Korperich H, Barth P, Esdorn H, Gieseke J, Meyer H. Noninvasive quantification of left-to-right shunt in pediatric patients: phase-contrast cine magnetic resonance imaging compared with invasive oximetry. Circulation 2001;103:2476–82.
5. Hundley WG, Li HF, Lange RA, Pfeifer DP, Meshack BM, Willard JE, Landau C, Willett D, Hillis LD, Peshock RM. Assessment of left-to-right intracardiac shunting by velocity-encoded, phase-difference magnetic resonance imaging. A comparison with oximetric and indicator dilution techniques. Circulation 1995;91:2955–60.
6. Arheden H, Holmqvist C, Thilen U, Hanseus K, Bjorkhem G, Pahlm O, Laurin S, Stahlberg R. Left-to-right cardiac shunts: comparison of measurements obtained with MR velocity mapping and with radionuclide angiography. Radiology 1999;211:453–8.
7. Diethelm L, Dery R, Lipton MJ, Higgins CB. Atrial-level shunts: sensitivity and specificity of MR in diagnosis. Radiology 1987;162:181–6.
8. Dinsmore RE, Wismer GL, Guyer D, Thompson R, Liu P, Stratemeier E, Miller S, Okada R, Brady T. Magnetic resonance imaging of the interatrial septum and atrial septal defects. Am J Roentgenol 1985;145:697–703.
9. Sakakibara M, Kobayashi S, Imai H, Watanabe S, Masuda Y, Inagaki Y. Diagnosis of atrial septal defect using magnetic resonance imaging. J Cardiol 1987;17:817–29.
10. Holmvang G, Palacios IF, Vlahakes GJ, Dinsmore RE, Miller SW, Liberthson RR, Block PC, Ballen B, Brady TJ, Kantor HL. Imaging and sizing of atrial septal defects by magnetic resonance. Circulation 1995;92:3473–80.
11. Beerbaum P, Korperich H, Esdorn H, Blanz U, Barth P, Hartmann J, Gieseke J, Meyer H. Atrial septal defects in pediatric patients: noninvasive sizing with cardiovascular MR imaging. Radiology 2003;228:361–9.
12. Durongpisitkul K, Tang NL, Soongswang J, Laohaprasitiporn D, Nanal A. Predictors of successful transcatheter closure of atrial septal defect by cardiac magnetic resonance imaging. Pediatr Cardiol 2004;25:124–30.
13. Mohrs OK, Petersen SE, Erkapic D, Rubel C, Schrader R, Nowak B, Fach WA, Kauczor HU, Voigtlaender T. Diagnosis of patent foramen ovale using contrast-enhanced dynamic MRI: a pilot study. AJR Am J Roentgenol 2005;184:234–40.
14. Van Praagh R, Geva T, Kreutzer J. Ventricular septal defects: how shall we describe, name and classify them? J Am Coll Cardiol 1989;14:1298–9.
15. Bol-Raap G, Weerheim J, Kappetein AP, Witsenburg M, Bogers AJ. Follow-up after surgical closure of congenital ventricular septal defect. Eur J Cardiothorac Surg 2003;24:511–5.
16. Kumar K, Lock JE, Geva T. Apical muscular ventricular septal defects between the left ventricle and the right ventricular infundibulum. Diagnostic and interventional considerations. Circulation 1997;95:1207–13.
17. Knauth AL, Lock JE, Perry SB, McElhinney DB, Gauvreau K, Landzberg MJ, Rome JJ, Hellenbrand WE, Ruiz CE, Jenkins KJ. Transcatheter device closure of congenital and postoperative residual ventricular septal defects. Circulation 2004;110:501–7.
18. Didier D, Higgins CB, Fisher MR, Osaki L, Silverman NH, Cheitlin MD. Congenital heart disease: gated MR imaging in 72 patients. Radiology 1986;158:227–35.
19. Lowell DG, Turner DA, Smith SM, Bucheleres GH, Santucci BA, Gresick RJ, Jr, Monson DO. The detection of atrial and ventricular septal defects with electrocardiographically synchronized magnetic resonance imaging. Circulation 1986;73:89–94.
20. Baker EJ, Ayton V, Smith MA, Parsons JM, Ladusans EJ, Anderson RH, Maisey MN, Tynan M, Fagg NL, Deverall PB. Magnetic resonance imaging at a high field strength of ventricular septal defects in infants. Br Heart J 1989;62:305–10.
21. Bremerich J, Reddy GP, Higgins CB. MRI of supracristal ventricular septal defects. J Comput Assist Tomogr 1999;23:13–5.
22. Yoo SJ, Lim TH, Park IS, Hong CY, Song MG, Kim SH. Defects of the interventricular septum of the heart: en face MR imaging in the oblique coronal plane. Am J Roentgenol 1991;157:943–6.
23. Yoo SJ, Kim YM, Choe YH. Magnetic resonance imaging of complex congenital heart disease. Int J Card Imaging 1999;15:151–60.
24. Sorensen TS, Korperich H, Greil GF, Eichhorn J, Earth P, Meyer H, Pedersen EM, Beerbaum P. Operator-independent isotropic three-dimensional magnetic resonance imaging for morphology in congenital heart disease: a validation study. Circulation 2004;110:163–9.
25. Mohiaddin RH, Underwood R, Romeira L, Anagnostopoulos C, Karwatowski, SP, Laney R, Somerville J. Comparison between cine magnetic resonance velocity mapping and first-pass radionuclide angiocardiography for quantitating intracardiac shunts. Am J Cardiol 1995;75:529–32.
26. Geva T, Greil GF, Marshall AC, Landzberg M, Powell AJ. Gadolinium-enhanced 3-dimensional magnetic resonance angiography of pulmonary blood supply in patients with complex pulmonary stenosis or atresia: comparison with x-ray angiography. Circulation 2002;106:473–8.
27. Geva T, Van Praagh S. Anomalies of the pulmonary veins. In: Allen HD, Gutgessel HP, Clark EB, Driscoll DJ, eds. Moss & Adams' Heart Disease in Infants, Children, and Adolescents. Philadelphia: Lippincott Williams & Wilkins, 2001:736–72.
28. Neill CA, Ferencz C, Sabiston DC, Sheldon H. The familial occurrence of hypoplastic right lung with systemic arterial supply and venous drainage "scimitar syndrome". Bull Johns Hopkins Hosp 1960;107:1–21.
29. Greil GF, Powell AJ, Gildein HP, Geva T. Gadolinium-enhanced three-dimensional magnetic resonance angiography of pulmonary and systemic venous anomalies. J Am Coll Cardiol 2002;39:335–41.
30. Prasad SK, Soukias N, Hornung T, Khan M, Pennell DJ, Gatzoulis MA, Mohiaddin RH. Role of magnetic resonance angiography in the diagnosis of major aortopulmonary collateral arteries

and partial anomalous pulmonary venous drainage. Circulation 2004;109:207–14.
31. Ferrari VA, Scott CH, Holland GA, Axel L, Sutton MS. Ultrafast three-dimensional contrast-enhanced magnetic resonance angiography and imaging in the diagnosis of partial anomalous pulmonary venous drainage. J Am Coll Cardiol 2001;37:1120–8.
32. Roos-Hesselink JW, Scholzel BE, Heijdra RJ, Spitaels SE, Meijboom FJ, Boersma E, Bogers AJ, Simoons ML. Aortic valve and aortic arch pathology after coarctation repair. Heart 2003;89:1074–7.
33. Konen E, Merchant N, Provost Y, McLaughlin PR, Crossin J, Paul NS. Coarctation of the aorta before and after correction: the role of cardiovascular MRI. Am J Roentgenol 2004;182:1333–9.
34. Campbell M. Natural history of coarctation of the aorta. Br Heart J 1970;32:633–40.
35. Bogaert J, Gewillig M, Rademakers F, Bosmans H, Verschakelen J, Daenen W, Baert AL. Transverse arch hypoplasia predisposes to aneurysm formation at the repair site after patch angioplasty for coarctation of the aorta. J Am Coll Cardiol 1995;26:521–7.
36. Parks, WJ, Ngo, TD, Plauth, WH, Bank, ER, Sheppard, SK, Pettigrew, RI, Williams, WH. Incidence of aneurysm formation after dacron patch aortoplasty repair for coarctation of the aorta: long-term results and assessment utilizing magnetic resonance angiography with three-dimensional surface rendering. J Am Coll Cardiol 1995;26:266–71.
37. Rao PS, Jureidini SB, Balfour IC, Singh GK, Chen SC. Severe aortic coarctation in infants less than 3 months: successful palliation by balloon angioplasty. J Invasive Cardiol 2003;15:202–8.
38. Corno AF, Botta U, Hurni M, Payot M, Sekairski N, Tozzi P, von Segesser LK. Surgery for aortic coarctation: a 30 years experience. Eur J Cardiothorac Surg 2001;20:1202–6.
39. Walhout RJ, Lekkerkerker JC, Ernst SM, Hutter PA, Plokker TH, Meijboom EJ. Angioplasty for coarctation in different aged patients. Am Heart J 2002;144:180–6.
40. Fawzy ME, Awad M, Hassan W, Al Kadhi Y, Shoukri M, Fadley F. Long-term outcome (up to 15 years) of balloon angioplasty of discrete native coarctation of the aorta in adolescents and adults. J Am Coll Cardiol 2004;43:1062–7.
41. Therrien J, Thorne SA, Wright A, Kilner PJ, Somerville J. Repaired coarctation: a “cost-effective” approach to identify complications in adults. J Am Coll Cardiol 2000;35:997–1002.
42. Simpson IA, Chung KJ, Glass RF, Sahn DJ, Sherman FS, Hesselink J. Cine magnetic resonance imaging for evaluation of anatomy and flow relations in infants and children with coarctation of the aorta. Circulation 1988;78:142–8.
43. Mendelsohn AM, Banerjee A, Donnelly LF, Schwartz DC. Is echocardiography or magnetic resonance imaging superior for precoarctation angioplasty evaluation? Cathet Cardiovasc Diagn 1997;42:26–30.
44. Rupprecht T, Nitz W, Wagner M, Kreissler P, Rascher W, Hofbeck M. Determination of the pressure gradient in children with coarctation of the aorta by low-field magnetic resonance imaging. Pediatr Cardiol 2002;23:127–31.
45. Prince MR, Narasimham DL, Jacoby WT, Williams DM, Cho KJ, Marx MV, Deeb GM. Three-dimensional gadolinium-enhanced MR angiography of the thoracic aorta. AJR Am J Roentgenol 1996;166:1387–97.
46. Krinsky GA, Rofsky NM, DeCorato DR, Weinreb JC, Earls JP, Flyer MA, Galloway AC, Colvin SB. Thoracic aorta: comparison of gadolinium-enhanced three-dimensional MR angiography with conventional MR imaging. Radiology 1997;202:183–93.
47. Masui T, Katayama M, Kobayashi S, Ito T, Seguchi M, Koide M, Nozaki A, Sakahara H. Gadolinium-enhanced MR angiography in the evaluation of congenital cardiovascular disease pre- and postoperative states in infants and children. J Magn Reson Imaging 2000;12:1034–42.
48. Bogaert J, Kuzo R, Dymarkowski S, Janssen L, Celis I, Budts W, Gewillig M. Follow-up of patients with previous treatment for coarctation of the thoracic aorta: comparison between contrast-enhanced MR angiography and fast spin-echo MR imaging. Eur Radiol 2000;10:1847–54.
49. Simpson IA, Chung KJ, Glass RF, Sahn DJ, Sherman FS, Hesselink J. Cine magnetic resonance imaging for evaluation of anatomy and flow relations in infants and children with coarctation of the aorta. Circulation 1988;78:142–8.
50. Fawzy ME, von Sinner W, Rifai A, Galal O, Dunn B, el-Deeb F, Zaman. Magnetic resonance imaging compared with angiography in the evaluation of intermediate-term result of coarctation balloon angioplasty. American Heart Journal 1993;126:1380–4.
51. Muhler EG, Neuerburg JM, Ruben A, Grabitz RG, Gunther RW, Messmer, von Bernuth BJ. Evaluation of aortic coarctation after surgical repair: role of magnetic resonance imaging and Doppler ultrasound. British Heart Journal 1993;70:285–90.
52. Riquelme C, Laissy JP, Menegazzo D, Debray MP, Cinqualbre A, Langlois J, Schouman-Claeys E. MR imaging of coarctation of the aorta and its postoperative complications in adults: assessment with spin-echo and cine-MR imaging. Magnetic Resonance Imaging 1999;17:37–46.
53. Godart F, Labrot G, Devos P, McFadden E, Rey C, Beregi JP. Coarctation of the aorta: comparison of aortic dimensions between conventional MR imaging, 3D MR angiography, and conventional angiography. Eur Radiol 2002;12:2034–9.
54. Stern HC, Locher D, Wallnofer K, Weber F, Scheid KF, Emmrich P, Buhlmeyer K. Noninvasive assessment of coarctation of the aorta: comparative measurements by two-dimensional echocardiography, magnetic resonance, and angiography. Pediatr Cardiol 1991;12:1–5.
55. Gutberlet M, Hosten N, Vogel M, Abdul-Khaliq H, Ehrenstein T, Amthauer H, Hoffmann T, Teichgraber U, Berger F, Lange P, Felix R. Quantification of morphologic and hemodynamic severity of coarctation of the aorta by magnetic resonance imaging. Cardiol Young 2001;11:512–20.
56. Mohiaddin RH, Kilner PJ, Rees S, Longmore DB. Magnetic resonance volume flow and jet velocity mapping in aortic coarctation. J Am Coll Cardiol 1993;22:1515–21.
57. Steffens JC, Bourne MW, Sakuma H, O’Sullivan M, Higgins CB. Quantification of collateral blood flow in coarctation of the aorta by velocity encoded cine magnetic resonance imaging. Circulation 1994;90:937–43.
58. Nielsen JC, Powell AJ, Gauvreau K, Marcus EN, Prakash A, Geva T. Magnetic resonance imaging predictors of coarctation severity. Circulation 2005;111:622–8.
59. Oshinski JN, Parks WJ, Markou CP, Bergman HL, Larson BE, Ku DN, Mukundan SJ, Pettigrew RI. Improved measurement of pressure gradients in aortic coarctation by magnetic resonance imaging. J Am Coll Cardiol 1996;28:1818–26.
60. Holmqvist C, Stahlberg F, Hanseus K, Hochbergs P, Sandstrom S, Larsson EM, Laurin S. Collateral flow in coarctation of the aorta with magnetic resonance velocity mapping: correlation to morphological imaging of collateral vessels. J Magn Reson Imaging 2002;15:39–46.
61. Araoz PA, Reddy GP, Tarnoff H, Roge CL, Higgins CB. MR findings of collateral circulation are more accurate measures of hemodynamic significance than arm-leg blood pressure gradient after repair of coarctation of the aorta. J Magn Reson Imaging 2003;17:177–83.
62. Julsrud PR, Breen JF, Felmlee JP, Warnes CA, Connolly HM, Schaff HV. Coarctation of the aorta: collateral flow assessment with phase-contrast MR angiography. AJR Am J Roentgenol 1997;169:1735–42.